PIER C

(Received 14 August 2025, Accepted 22 September 2025, Scheduled 29 September 2025)

Design of Multi-Resonator Coupled Duplexer Based on Electromagnetic Coupling Path Separation

Mingxin Liu[1,2,*], Jialin Zhang[1], Yan Zhang[1], Qunjie Zhang[1], and Lin Fu[1]

[1]Chengdu Aeronautic Polytechnic University, Chengdu 610100, China
[2]University of Electronic Science and Technology of China, Chengdu 611731, China

ABSTRACT: In RF front-end circuits, the miniaturization and high-performance integration of duplexer remain critical challenges for 5G communication and IoT devices. A microstrip duplexer design scheme is proposed based on electric and magnetic coupling path separation and dual-mode characteristics. Through the collaborative design of second-order uniform impedance resonators and dual-mode T-shaped resonators, the design achieves signal separation for dual frequency bands at 2.4 GHz and 3.6 GHz. The design forms the electric coupling path via edge-gap coupling of rectangular split-ring resonators and realizes magnetic coupling path through vias. By independently regulating electric and magnetic coupling strengths, eight transmission zeros are introduced on both sides of the dual passbands, significantly enhancing out-of-band suppression and port isolation. The simulation results show that the passband insertion loss is less than or equal to 1.9 dB. Due to machining tolerances, the measured center frequencies shift to 2.04 and 3.48 GHz, while the out-of-band rejection remains better than 39 dB, validating the engineering adaptability of the design. This scheme achieves high-performance integration of RF front-ends in a compact architecture through the coordinated regulation of multiple transmission zeros and coupling path separation technology, providing a solution for wireless communication devices.

1. INTRODUCTION

In radio frequency (RF) front-end circuits, duplexer serves as a core component for separating transmitted and received signals at the antenna, directly influencing the spectral efficiency and anti-interference capability of wireless communication systems. A duplexer typically consists of two cascaded bandpass filters and must achieve low insertion loss and high port isolation within target frequency bands [1–4]. With the widespread application of 2.4 GHz and 3.6 GHz frequency bands, duplexer design faces the dual challenges of insufficient transmission zero control accuracy and redundant circuit size [5–7].

It is difficult to achieve coordinated control of multiple transmission zeros and reduce out of band suppression and duplexer isolation in existing duplexer design schemes such as ordinary T-shaped resonators [8], defected ground slotline resonators [9], slotline-loaded ring resonators [10], dual-mode stub resonators [11], and hybrid electromagnetic coupling resonators [12]. Although coupling additional resonators into an all-resonator-based duplexer can introduce transmission zeros, it comes at the cost of a significantly larger circuit size [13]. A dual-band dual-polarized substrate integrated waveguide (SIW) cavity-backed antenna-duplexer achieves off-body communication compatibility by combining an antenna with a duplexer, but its SIW cavity structure results in a large footprint and high insertion loss [14]. Another work proposes bandwidth-improved half mode SIW (HMSIW) resonator-based filtennas for single/dual-channel networks, which integrates filtering and radiation functions but lacks independent regulation of transmission zeros, leading to limited out-of-band suppression [15].

To address the above mentioned issues, a design scheme for a microstrip duplexer with multi-coupled resonators is proposed based on electric and magnetic coupling path separation and dual-mode characteristics. This design employs a multi-resonator architecture, achieving controllable generation of multiple transmission zeros through an optimized coupling mechanism. Within this architecture, some transmission zeros can be independently controlled via electric and magnetic coupling. Simulation results show that the passband insertion loss is less than or equal to 2.15 dB, the port isolation greater than 38 dB, and the circuit size of the lower frequency band only $0.66\lambda_g \times 0.15\lambda_g$, where λ_g is the waveguide wavelength. By introducing a multi-transmission zero mechanism, the duplexer controls the insertion loss within 1.9 dB and improves the port isolation to more than 38 dB while maintaining a compact size, achieving high-performance integration of RF front-end components.

2. THE DUPLEXER DESIGN PRINCIPLE

The core unit of the multi-resonator coupled duplexer employs second-order uniform impedance resonators, achieving dual-band signal transmission through separated electromagnetic coupling paths. The structure uses a dual-mode T-shaped resonator as the feeding network, whose even and odd mode characteristics correspond to 2.4 GHz and 3.6 GHz, respectively. Two sets of separated electromagnetic coupling resonators with different sizes are designed by the physical size of $\lambda_g/4$, en-

* Corresponding author: Mingxin Liu (lmx0951@163.com).

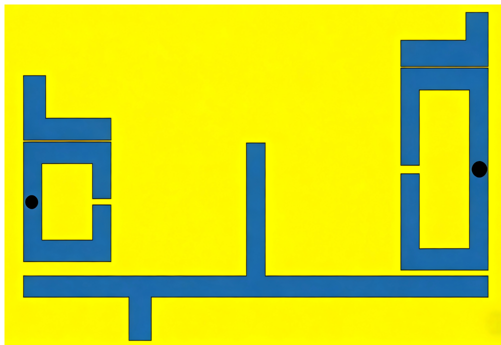

FIGURE 1. Structure diagram of duplexer.

suring strict matching between the feeding structure and center frequency of the resonator. The duplexer establishes an electrical coupling path through end-gap coupling of rectangular split-ring resonators, while electromagnetic coupling is introduced via vias, as illustrated in Fig. 1. This design with separated electrical/magnetic coupling paths provides a structural foundation for independent control of transmission zeros.

The electric coupling path relies on capacitive energy storage between microstrip edges. During signal coupling, the electric field dominates, and the transmitted signal maintains a 0° phase shift (no phase inversion). The magnetic coupling path relies on inductive energy storage. Vias act as distributed inductors, and the magnetic field interaction during coupling causes a 180° phase shift (half-wavelength phase inversion) of the transmitted signal. When the amplitudes of the signals from the two paths are equal, the 0° and 180° phase difference leads to complete destructive interference when this interference frequency point is the transmission zero.

The topological coupling structure of the duplexer is shown in Fig. 2, where P1 is the input port, and P2 and P3 are the two output ports respectively. R1-R2 and R5-R6 are two sets of second-order separated electromagnetic coupling resonators with different center frequencies, while R3 and R4 correspond to the odd mode and even mode of the T-shaped resonator, respectively. Signals are output through the first channel and the second channel via two coupling paths of R1-R2-R3 and R4-R5-R6, respectively.

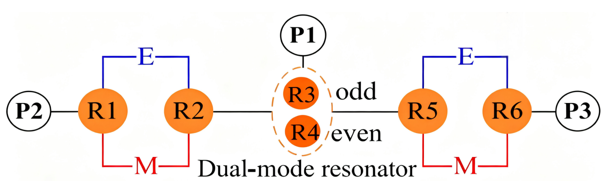

FIGURE 2. Coupling topology of duplexer.

3. DESIGN STEPS OF DUPLEXER

The duplexer is fabricated on a Rogers 6010 dielectric substrate with a relative permittivity of 10.2 and a thickness of 1.27 mm. The specific structural parameters are shown in Fig. 3. This substrate selection can effectively suppress dielectric loss in the high-frequency band, meeting the operational requirements for the 2.4 GHz and 3.6 GHz.

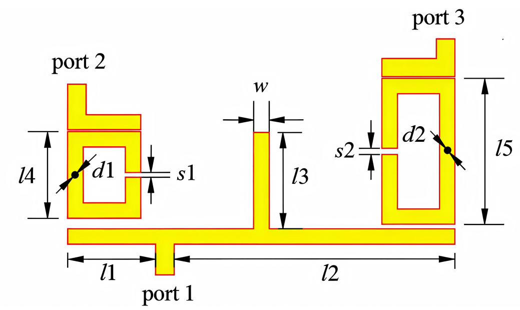

FIGURE 3. Structure parameter diagram of duplexer.

The structure of the T-shaped dual-mode resonator is shown in Fig. 4(a), while the equivalent transmission line circuits for its odd-mode and even-mode are presented in Figs. 4(b) and (c), respectively. Based on transmission line theory, the electrical lengths of the even-mode and odd-mode are $\theta_a + \theta_b$ and θ_a, with corresponding characteristic impedances of Z_a and Z_b. According to microwave network theory, the input admittance of the odd-mode Y_{in}^o and even-mode Y_{in}^e can be expressed as

$$Y_{in}^o = j\frac{\tan\theta_a}{Za} \tag{1}$$

$$Y_{in}^e = j\frac{Z_a \tan\theta_b + Z_b \tan\theta_a}{Z_a(Z_b - \tan\theta_a \tan\theta_b)} \tag{2}$$

By adjusting the resonator geometric parameters, the resonant frequencies of the odd-mode and even-mode are configured to 2.4 GHz and 3.6 GHz, respectively, with the corresponding even-mode length 20.04 mm and odd-mode length 12.7 mm. As can be seen from Fig. 4, the even-mode length and odd-mode length can be computed by $(l1+l2+w)/2+l3+w$ and $(l1 + l2 + w)/2$, respectively. To be compatible with the standard printed circuit board (PCB) drilling process, the initial coupling gap $s2$ is set to 0.4 mm, and the via diameter $d2$ is 0.42 mm. By using the advanced design system (ADS) Linecalc tool, the physical dimensions (in mm) of the resonator in Fig. 3 are initially calculated and further optimized, resulting in detailed dimensions as shown in Table 1.

TABLE 1. Parameters of the duplexer.

Parameter	Value	Parameter	Value
$l1$	5.8 mm	$l2$	18.6 mm
$l3$	6.34 mm	$l4$	5.8 mm
$l5$	9.6 mm	w	1 mm
$d1$	0.38 mm	$d2$	0.42 mm
$s1$	0.2 mm	$s2$	0.4 mm

The current distribution of the duplexer obtained by software simulation is shown in Fig. 5. It can be clearly seen that at the operating frequency of 2.4 GHz, signals mainly propagate through resonators R1-R2 and odd-mode path of the T-shaped resonator. At this time, the odd-mode current shows a strong coupling state in the vertical arm of the T-structure. The current distribution in the 3.6 GHz band is concentrated on resonators

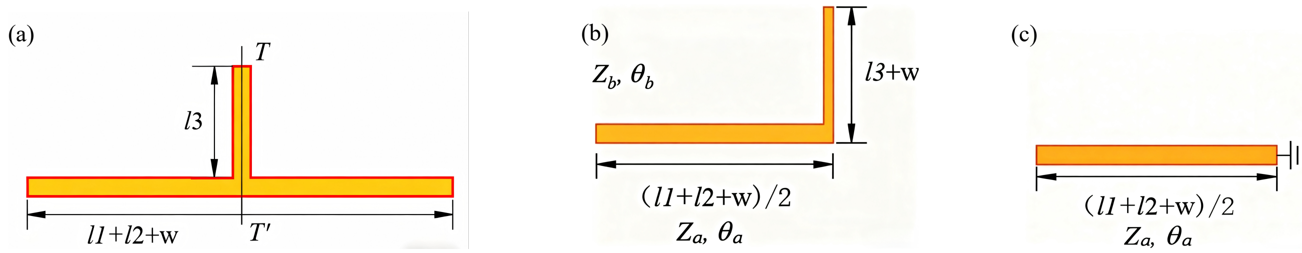

FIGURE 4. Even-odd mode equivalent circuits of T-shaped resonator. (a) T-shaped resonator, (b) even-mode equivalent circuit, (c) odd-mode equivalent circuit.

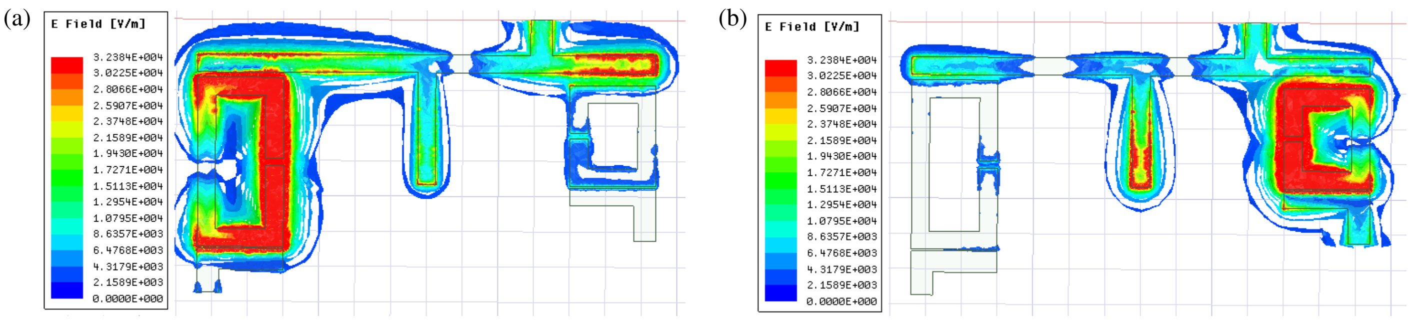

FIGURE 5. Current distribution of duplexer. (a) Electric field distribution at 2.4 GHz, (b) electric field distribution at 3.6 GHz.

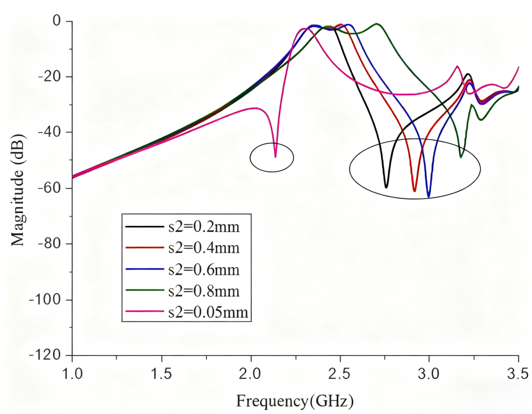

FIGURE 6. Curve of transmission zero 1 versus parameter $s2$.

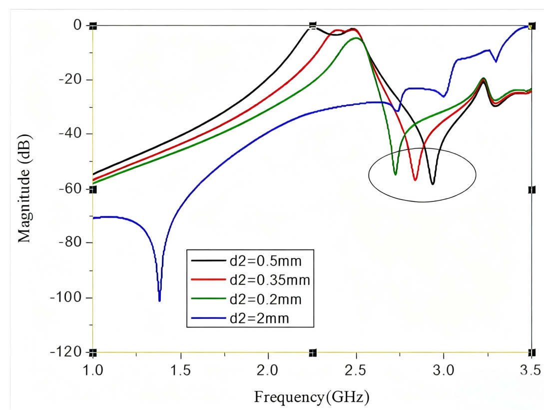

FIGURE 7. Curve of transmission zero 1 versus parameter $d2$.

R5-R6 and the even-mode path of the T-shaped resonator, and the even-mode current forms a symmetric distribution in the horizontal arm of the T-structure. This mode separation characteristic is in good agreement with the theoretical design, verifying the feasibility of the duplexer to achieve independent regulation of dual bands through even-odd mode resonance.

From the perspective of microwave equivalent circuits, the gap between metal microstrips can be equivalent to a distributed capacitance, and its width directly reflects the electric coupling strength. The metallized via is equivalent to a distributed inductor, and the diameter size represents the magnetic coupling strength. For the 2.4 GHz channel, as can be seen from Fig. 6, when the coupling gap $s2$ increases from 0.2 mm to 0.8 mm, the electric coupling strength weakens while the magnetic coupling remains unchanged, and the transmission zero 1 shifts to the high-frequency stopband away from the center frequency of the passband. At this time, the phase cancellation point of electric/magnetic coupling occurs in the higher frequency band. When $s2$ is reduced to 0.05 mm, the electric coupling strength exceeds the critical value, and transmission zero 1 moves from the high-frequency stopband to the low-frequency stopband, which is due to the frequency shift reversal of the phase cancellation point of electric/magnetic coupling caused by excessive electric coupling.

This shift of transmission zero 1 is inherently driven by the variation of electric field intensity at the edge gap of the rectangular split-ring resonators. As $s2$ decreases, the gap between split-ring resonator edges narrows, leading to increased concentration of electric field lines at the gap. This enhanced electric field intensity strengthens the electric coupling effect, and the electric field reaches a critical strength in $s2 = 0.05$ mm that reverses the phase cancellation frequency of electric and magnetic coupling, thus shifting transmission zero 1 to the low-frequency stopband. Conversely, a larger $s2$ disperses the elec-

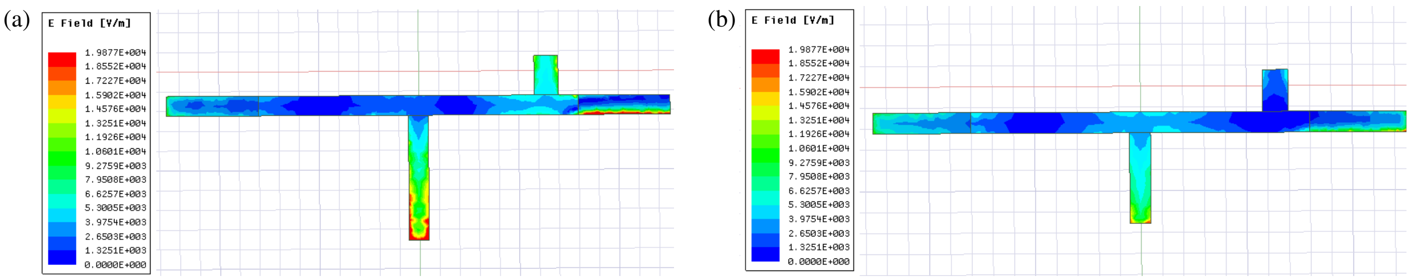

FIGURE 8. Electric field intensity of T-shaped resonator at different $l3$ lengths. (a) $l3$ is longer, (b) $l3$ is shorter.

tric field at the gap, weakens electric coupling, and moves the phase cancellation point to the high-frequency band.

Further analysis of the simulation results in Fig. 7 reveals that as the via diameter $d2$ increases from 0.5 mm to 2 mm, the magnetic coupling strength decreases with the expanding via size, while the electric coupling strength remains constant. During this process, transmission zero 1 moves from the high-stopband closer to the passband center frequency, and the cancellation of electric and magnetic couplings occurs at a lower frequency than before. When $d2$ increases to 2.0 mm, transmission zero 1 lies in the lower stopband and deviates from the center frequency. This phenomenon indicates that the position of transmission zero 1 is determined by the hybrid electromagnetic coupling effect of the larger second-order separated electromagnetic coupling resonator. Similar to 2.4 GHz passband, transmission zero 2 is determined by the hybrid electromagnetic coupling of the smaller second-order separated electromagnetic coupling resonator in 3.6 GHz, exhibiting a behavior analogous to that of transmission zero 1.

The weakening of magnetic coupling with increasing $d2$ is rooted in the variation of magnetic field intensity around metallized vias. A smaller $d2$ (e.g., 0.2 mm) restricts the current path of the via, concentrating the magnetic field around the via and strengthening magnetic coupling. As $d2$ increases to 2 mm, the widened current path disperses the magnetic field, reducing magnetic coupling strength. This weakening reduces the phase cancellation frequency of electric and magnetic coupling.

Specifically, transmission zero 1 in 2.4 GHz is generated when the hybrid electromagnetic coupling meets the equal amplitude opposite phase condition. The electric coupling strength (controlled by $s2$) determines the amplitude of the $0°$ phase signal. A smaller $s2$ narrows the gap, enhancing capacitive coupling and increasing the signal amplitude. The magnetic coupling strength (controlled by $d2$) determines the amplitude of the $180°$ phase signal. A smaller $d2$ reduces the via's current path, enhancing inductive coupling and increasing the signal amplitude. Under the conditions of strong electrical and magnetic coupling, when the amplitudes of the two signals are equal, destructive interference occurs at the $0°/180°$ phase, forming transmission zero 1 in the low-frequency stopband. If the equal amplitude condition is broken, the interference point will move accordingly.

As shown in Fig. 8, the magnetic field intensity of the T-shaped dual-mode resonator adjacent to the small second-order separated electromagnetic coupling resonator increases with the increase of parameter $l3$. This magnetic field variation directly alters the electromagnetic coupling coefficient of the R4-R5-R6 resonator group, causing transmission zero 3 to migrate from the low-frequency stopband to the high-frequency stopband when electric and magnetic couplings cancel each other out. The relationship between transmission zero 3 and parameter $l3$ is illustrated in Fig. 9. It can be seen that for the 3.6 GHz passband, when $l3$ increases from 4 mm to 6.34 mm, transmission zero 3 moves from the lower stopband closer to the center frequency. When $l3$ exceeds 7.0 mm, transmission zero 3 shifts from the lower stopband to the higher stopband. This phenomenon confirms that transmission zero 3 is determined by the coupling effect between the even mode of the T-shaped resonator and the small second-order separated electromagnetic coupling resonator, complementing the mechanism where transmission zeros 1 and 2 are dominated by separated electromagnetic coupling resonators as analyzed earlier. Further studies show that parameter $l3$ significantly affects only the transmission zeros of the 3.6 GHz upper channel, with little effect on the lower channel.

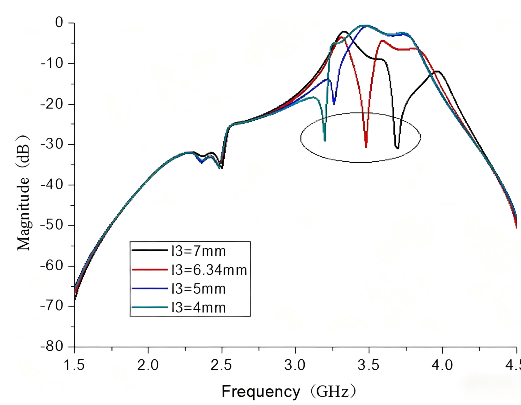

FIGURE 9. Curve of transmission zero 3 versus parameter $l3$.

Transmission zero 3 follows the same phase interference admittance deviation mechanism but involves the even mode of the T-shaped resonator. The even mode provides the base admittance Y_{in}^{e}, and the small second-order resonators introduce additional electromagnetic coupling. Parameter T' adjusts the even-mode's electrical length $\theta_a + \theta_b$, which changes Y_{in}^{e}. When $l3$ increases from 4 mm to 7 mm, $\theta_a + \theta_b$ approaches $\pi/2$, increasing $|Y_{in}^{e}|$, which alters the balance among Y_{in}^{e}, capacitive admittance, and inductive admittance.

TABLE 2. Performance parameter comparison of duplexers.

Reference	$f1/f2$	Isolation (dB)	Transmission zeros	Size at $f1$ (mm^2)	Size at $f2$ (mm^2)	Minimum element spacing (mm)
20	1.95/2.14	44/36	2	0.56×0.38	0.61×0.42	1.0
21	1.1/1.3	33/26	2	0.86×0.82	1.2×0.97	0.2
22	1.95/2.14	32/37	5	0.38×0.36	0.42×0.4	0.2
16	2.4/3.5	45/42	7	0.59×0.48	0.86×0.7	0.2
19	1.73/2.25	35.9/35.5	5	0.24×0.62	0.42×0.9	0.23
This Work	2.45/3.6	43/42	8	0.51×0.25	0.77×0.37	0.2

Note: All size data in this table are based on the waveguide wavelength λ_g.

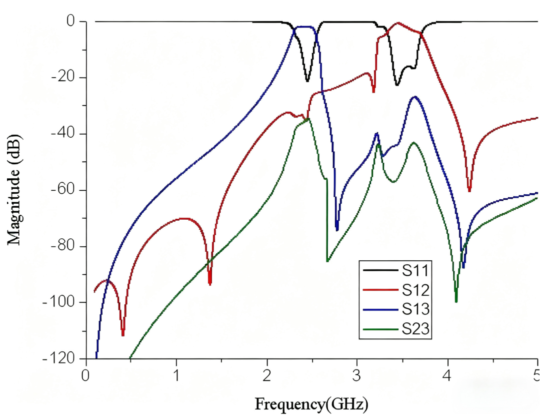

FIGURE 10. Simulation results of parameter S.

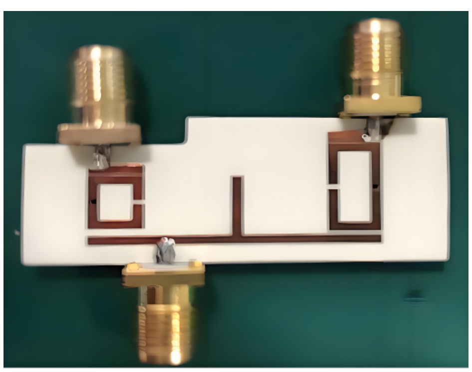

FIGURE 11. Physical prototype of duplexer.

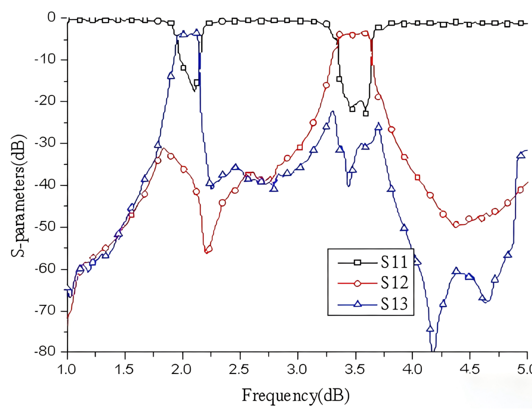

FIGURE 12. Measured results of parameter S.

4. SIMULATION AND MEASUREMENT RESULT

4.1. Simulation Results

To verify the design feasibility, the duplexer was simulated using simulation software, and the results are shown in Fig. 10. When the passband S_{11} of the duplexer is less than -10 dB, the corresponding frequency range is 2.4 GHz–2.56 GHz and 3.24 GHz–3.38 GHz. Eight transmission zeros are introduced on both sides of each passband, effectively improving the passband rectangularity coefficient and channel isolation. The out-of-band rejection of the two passbands is 38 dB, and the isolation between the two passbands is better than 42 dB, verifying the effectiveness of the electric and magnetic coupling path separation design for multi-transmission zero regulation.

4.2. Measurement Results

The fabricated duplexer based on a Rogers 6010 substrate is shown in Fig. 11, with SMA connectors for feeding connections. The measured S-parameters are presented in Fig. 12. Measurement data show that the lower channel has a center frequency of 2.04 GHz with an absolute bandwidth covering 1.9–2.16 GHz, while the upper channel has a center frequency of 3.48 GHz and a bandwidth of 3.36–3.64 GHz. Transmission zeros appear at 2.3 GHz and 4.3 GHz, with out-of-band rejection of both passbands better than 39 dB. The offset between measured and simulated center frequencies is mainly caused by processing tolerances and connector parasitic parameters. Despite frequency shift, the out-of-band rejection and isolation indices exceed simulation results, demonstrating the design's adaptability to engineering implementation.

4.3. Results and Discussion

The designed duplexer achieves a compact circuit layout of 24.8 mm × 12.2 mm $(0.51\lambda_g \times 0.25\lambda_g)$ in the lower frequency range, which has significant performance advantages compared to other duplexers using microstrip line technology, as shown in Table 2. It is evident that the designed circuit size is reduced by 40%, 82%, 7%, and 55% respectively compared to [14–17] at the low center frequency $f1$ of the first resonance. At the second resonant high-center frequency $f2$, the size is reduced by 75% and 43% compared to [18] and [19], respectively. The duplexer achieves an isolation of 43/42 dB in the $f1/f2$ frequency bands, outperforming the 44/36 dB in [16] and 32/37 dB in [18]. Meanwhile, the introduction of 8 transmission zeros effectively enhances the out-of-band rejection capability. The design of minimizing element spacing enables stronger electric coupling in a compact area, which is a key to generating 8 transmission zeros without increasing circuit size, highlighting the design's uniqueness in miniaturization and integration density.

5. CONCLUSION

A design scheme for a microstrip duplexer with multi-coupled resonators based on electric and magnetic coupling path separation and dual-mode characteristics is proposed. The design achieves precise positioning of multiple transmission zeros by independently regulating electric and magnetic coupling paths, effectively improving passband selectivity. The duplexer employs a dual-mode T-shaped resonator as the feeding structure, reduces the number of resonators using even-odd mode characteristics, and meets the miniaturization requirements of RF front-ends by combining a compact $\lambda_g/4$ resonator size design. Simulation results show that the duplexer has a passband insertion loss less than 1.9 dB and port isolation exceeding 38 dB in 2.4 and 3.6 GHz.

This design supports supplementary downlink transmission in 5G NR systems, where the 3.6 GHz mid-band meets urban area coverage needs, and the 2.4 GHz band serves as a reliable fallback for indoor signal penetration, ensuring stable uplink/downlink signal separation. In internet of things (IoT) end devices, its miniaturized structure and 2.4 GHz band compatibility enable direct integration with Wi-Fi 6/Bluetooth Low Energy modules, reducing the complexity of additional frequency conversion circuits. In the future, within the framework of the current design, a third-order resonator will be introduced to expand the 3.6 GHz passband bandwidth to 400 MHz, so as to meet the requirements of 5G communication for wider channels. Additionally, based on the existing dual-mode T-shaped resonator structure, the duplexer can be integrated with a filtering power divider to develop a single-chip RF front-end module, further enhancing the miniaturization level for IoT applications.

ACKNOWLEDGEMENT

This work was supported in part by the Longquanyi District New Economy and Science and Technology Plan Project — Research on the Development Strategy of Low-Altitude Economic Industry in Longquanyi District Supported by Drones (Grant No. ZRT0624177), High-Level Talent Scientific Research Start-up Funding Project (Grant No. ZZX0624068), and Project of Research Center for Chengdu Aerospace Industry Development and Cultural Construction (Grant No. CAIACDRCXM2025-48).

REFERENCES

[1] Yu, Y., Y. Wang, T. Skaik, T. Starke, X. Shang, M. J. Lancaster, P. Hunyor, P. G. Huggard, H. Wang, M. Harris, M. Beardsley, and Q. S. Cheng, "D-band waveguide diplexer fabricated using micro laser sintering," *IEEE Transactions on Components, Packaging and Manufacturing Technology*, Vol. 12, No. 9, 1446–1457, Sep. 2022.

[2] Wang, H., H. Shi, W. E. I. Sha, Z. Lan, F. Gao, X. Chen, and A. Zhang, "Design of high-isolation topological duplexer utilizing dual-edge state topological waveguides," *IEEE Transactions on Antennas and Propagation*, Vol. 72, No. 11, 8802–8809, Nov. 2024.

[3] Yao, C., W. Ma, and H. Lin, "A W-band high intermediate-frequency subharmonic mixer utilizing a novel T-type duplexer," *IEEE Microwave and Wireless Technology Letters*, Vol. 35, No. 2, 233–236, Feb. 2025.

[4] Seong, M., J. Kim, and Y. Eo, "SAW device with reactive reflector for integrated SAW RF duplexer area minimization," *IEEE Transactions on Electron Devices*, Vol. 71, No. 10, 6312–6319, Oct. 2024.

[5] Zhou, L., J. Jiang, W. Zhang, P. K. J. Wong, B. Xia, D. Zhang, X. Bai, and X. Lu, "Design of high order HTS duplexer based on SIR structure," *IEEE Transactions on Applied Superconductivity*, Vol. 33, No. 4, 1–8, Jun. 2023.

[6] Khani, A. A. M., M. Fouladian, and J. Mazloum, "Multi layers THz duplexer based on combined graphene patterns," *Solid State Communications*, Vol. 360, 114974, Feb. 2023.

[7] Hsiao, M.-J. and C. Nguyen, "25–53 GHz ultra-wideband high-isolation passive balanced duplexer on 0.18-μm BiCMOS for 5G applications," *IET Microwaves, Antennas & Propagation*, Vol. 14, No. 15, 1960–1968, Dec. 2020.

[8] Ahmad, W. and D. Budimir, "Dual-band filtenna array for WLAN applications," *Microwave and Optical Technology Letters*, Vol. 58, No. 2, 477–481, Feb. 2016.

[9] Lin, C.-K. and S.-J. Chung, "A filtering microstrip antenna array," *IEEE Transactions on Microwave Theory and Techniques*, Vol. 59, No. 11, 2856–2863, Nov. 2011.

[10] Iqbal, A., J. J. Tiang, C. K. Lee, and B. M. Lee, "Tunable substrate integrated waveguide diplexer with high isolation and wide stopband," *IEEE Microwave and Wireless Components Letters*, Vol. 29, No. 7, 456–458, Jul. 2019.

[11] Zhang, S., X.-D. Fu, T. Wang, F.-L. Liu, H.-T. Wang, and H. Liu, "Quasi quarter SIW-mode resonator and its application to sierpinski fractal filter design," *Microwave and Optical Technology Letters*, Vol. 58, No. 5, 1176–1179, May 2016.

[12] Deslandes, D. and K. Wu, "Single-substrate integration technique of planar circuits and waveguide filters," *IEEE Transactions on Microwave Theory and Techniques*, Vol. 51, No. 2, 593–596, Feb. 2003.

[13] Chaturvedi, D., A. Kumar, and A. A. Althuwayb, "A dual-band dual-polarized SIW cavity-backed antenna-duplexer for off-body communication," *Alexandria Engineering Journal*, Vol. 64, 419–426, Feb. 2023.

[14] Kumar, A., D. Chaturvedi, and A. A. Khan, "Bandwidth-improved HMSIW resonator based filtennas for single/dual channel network," in *2021 IEEE Indian Conference on Antennas and Propagation (InCAP)*, 502–505, Jaipur, Rajasthan, India, India, 2021.

[15] Wang, H.-Y., G. H. Li, Y.-D. Wu, W. Yang, and T. Mou, "A novel triple-band filter based on triple-mode substrate integrated waveguide," *Progress In Electromagnetics Research Letters*, Vol. 58, 59–65, 2016.

[16] Xiao, J.-K., M. Zhu, Y. Li, L. Tian, and J.-G. Ma, "High selective microstrip bandpass filter and diplexer with mixed electromagnetic coupling," *IEEE Microwave and Wireless Components Letters*, Vol. 25, No. 12, 781–783, Dec. 2015.

[17] Song, K., Y. Zhou, Y. Chen, A. M. Iman, S. R. Patience, and Y. Fan, "High-isolation diplexer with high frequency selectivity using substrate integrate waveguide dual-mode resonator," *IEEE Access*, Vol. 7, 116 676–116 683, 2019.

[18] Gao, Y., S. Wen, J. Yuan, and X. Xu, "Design of interdigital-filter based diplexer with high isolation and wideband," *High Power Laser and Particle Beams*, Vol. 31, No. 8, 084101, 2019.

[19] Zhu, C. and J. Zhang, "Design of diplexer-integrated filtering power divider with high isolation," *Microwave and Optical Technology Letters*, Vol. 61, No. 11, 2607–2613, Nov. 2019.

[20] Chuang, M.-L. and M.-T. Wu, "Microstrip diplexer design using common T-shaped resonator," *IEEE Microwave and Wireless Components Letters*, Vol. 21, No. 11, 583–585, Nov. 2011.

[21] Chen, D., L. Zhu, H. Bu, and C. Cheng, "A novel planar diplexer using slotline-loaded microstrip ring resonator," *IEEE Microwave and Wireless Components Letters*, Vol. 25, No. 11, 706–708, Nov. 2015.

[22] Guan, X., F. Yang, H. Liu, and L. Zhu, "Compact and high-isolation diplexer using dual-mode stub-loaded resonators," *IEEE Microwave and Wireless Components Letters*, Vol. 24, No. 6, 385–387, Jun. 2014.